Treating muscle and brain alike: benefits of GSK3 inhibition in *mdx* mice

Bianca M. Marcella[a1,2], Emily N. Copeland[a1,2,3], Sophie I. Hamstra[a1,2], Briana L. Hockey[1,2], Jessica L. Braun[1,2,3], Mia S. Geromella[1,2], Kennedy C. Whitley[1,2], Colton J.F. Watson[4], Bradley J. Baranowski[3,4], Lucas A. Maddalena[5], Ahmad Mohammad[3,4], Sebastian Silvera[1,2], Ryan W. Baranowski[1,2], Evelyn C. Ochoa[1,2,3], Luc Wasilewicz[1,2], Riley E.G. Cleverdon[1,2], Shawn Beaudette[1,2], Rene Vandenboom[1,2], Brian D. Roy[1,2], Jeffrey A. Stuart,[5] Adam J. MacNeil[3], Rebecca E.K. MacPherson[3,4*], Val A. Fajardo[1,2,4,6*]

[a] These authors contributed equally

[1] Department of Kinesiology, Brock University, St. Catharines, ON, Canada
[2] Centre for Bone and Muscle Health, Brock University, St. Catharines, ON, Canada
[3] Centre for Neurosciences, Brock University, St. Catharines, ON, Canada
[4] Department of Health Sciences, Brock University, St. Catharines, ON, Canada
[5] Department of Biological Sciences, Brock University, St. Catharines, ON, Canada
[6] Lead contact

*Corresponding authors:

Val A. Fajardo, PhD
Assistant Professor
Canada Research Chair (Tier II)
Department of Kinesiology
Brock University
St. Catharines, ON
L2S 3A1
vfajardo@brocku.ca

Rebecca E.K. MacPherson, PhD
Associate Professor
Department of Health Sciences
Brock University
St. Catharines, ON
L2S 3A1
rmacpherson@brocku.ca

Summary

In addition to progressive muscle wasting and weakness, many patients living with Duchenne muscular dystrophy (DMD) will experience cognitive decline, which further compromises their quality of life. Here, we questioned whether inhibiting glycogen synthase kinase 3 (GSK3) in the DBA/2J *mdx* mouse model of DMD could benefit both muscle and brain health. Short-term treatment with the clinically advanced GSK3 inhibitor, tideglusib, reduced skeletal and cardiac muscle necrosis, improving force production and diastolic function. Similar benefits were found when GSK3 inhibition via lithium supplementation was combined with voluntary wheel running. In the brain, GSK3 was found to be overactive in the hippocampus from *mdx* mice; and inhibiting GSK3 improved cognitive function. Further, this result was associated with reduced beta-secretase activity and increased clearance of β-amyloid. Altogether, our findings reveal GSK3 inhibition as a potential therapy for DMD – one aimed at enhancing muscle and brain health and overall quality of life.

Highlights

- Tideglusib treatment lowered muscle necrosis and improved cardiac and skeletal muscle function
- Combined effects of voluntary wheel running and lithium supplementation improved skeletal and cardiac muscle function despite running significantly less
- GSK3 inhibition shifts brain biochemistry away from an Alzheimer's-like pathology in *mdx* mice and improves cognitive function
- GSK3 inhibition can treat both muscles and brain and could potentially improve the quality of life of those living with DMD

Introduction

Duchenne muscular dystrophy (DMD) is a severe X-linked muscle wasting disorder that affects 1 in 5,000 males worldwide[1]. It is caused by the complete absence of functional dystrophin, which is a structural protein that provides membrane stability to muscle throughout their strenuous contraction-relaxation cycles. Without dystrophin, muscle integrity is compromised. This leads to progressive muscle wasting and weakness, and patients with DMD are often wheelchair-bound and present with severe cardiomyopathy by their teenage years[2]. There is no cure for DMD and despite recent advances in disease management, the average lifespan for an individual with DMD ranges from 20-30 years as they unfortunately succumb to cardiorespiratory failure[3].

In addition to muscle, a substantial proportion of boys living with DMD (30-40%) present with cognitive impairments and neurobehavioral changes such as lowered intelligence quotient (IQ) scores (<70)[4] and reading and learning deficits[5]. Combined, impaired muscle and cognitive function can lower one's quality of life; and improving both muscle and brain pathology can enhance the life of those suffering from DMD. Therefore, exploring the cellular mechanisms that underpin dystrophic pathology in both muscle and brain is important as it may reveal novel and universal therapeutic targets and intervention strategies.

Glycogen synthase kinase 3 (GSK3) is a serine/threonine (Ser/Thr) kinase that was first identified for its role in regulating glycogen synthase in muscle but is now known to phosphorylate more than 100 substrates all over the body[6]. There are two isoforms of GSK3, GSK3α and GSK3β, with the latter being the most expressed and active isoform found within muscle[7] and brain[8]. GSK3 can be inhibited via Ser phosphorylation (Ser21 on GSK3α and Ser9 on GSK3β), which prevents GSK3 from binding with its downstream targets[6]. In muscle, the inhibition of GSK3 promotes muscle mass via an increase in protein synthesis and myoblast fusion, and a decrease in proteolytic

degradation (for review see ref[9]). Furthermore, we and others have shown that the inhibition of GSK3 in skeletal muscle can increase the proportion of type I and IIA oxidative muscle fibres by activating the transcription factor, nuclear factor of activated T cells (NFAT)[10,11]. This is important in the context of DMD since this disease primarily affects the type II glycolytic fibers[12,13]; and therefore, promoting the oxidative fibres can attenuate dystrophic pathology[12,14-16].

In the brain, the inhibition of GSK3 has been viewed as a viable therapeutic strategy for many neurodegenerative diseases such as Parkinson's and Alzheimer's disease[17]. Recently, we identified an Alzheimer's-like pathology in young (10-12 week old) DBA/2J (D2) *mdx* mice, where these mice displayed spatial memory deficits and an unfavourable shift in brain biochemistry towards the production of β-amyloid peptides when compared with healthy wild-type (WT) mice[18]. In patients with DMD, the severity of cognitive dysfunction was found to be linked with increased levels of circulating β-amyloid peptides, and was suggested to be the cause of brain damage in these patients[19]. GSK3 is a well-established pathological player in Alzheimer's disease where its overactivation can increase the content and activation of beta-secretase 1 (BACE1), which is the rate-limiting step in amyloidogenesis[20]. Thus, GSK3 inhibition in DMD boys may reduce circulating β-amyloid peptides while also improving muscle health.

Here, we investigated the effects of inhibiting GSK3 in the D2 *mdx* mouse model. We first examined the effects of short-term treatment with tideglusib, which is the most clinically advanced GSK3 inhibitor currently being tested for other diseases and conditions[21,22]. Next, we investigated the combined effects of voluntary wheel running (VWR) and GSK3 inhibition via lithium (Li) supplementation. VWR improves both muscle and brain health in various mouse models[23-25]; and therefore, we sought to determine whether these benefits could be amplified with GSK3 inhibition.

RESULTS

Tideglusib treatment reduces muscle necrosis, improves muscle contractility, and prevents diastolic dysfunction

We first determined whether GSK3 content and activation status, as indicated by the levels of inhibitory Ser9 phosphorylation, would be different in D2 *mdx* mice compared with WT. Across the extensor digitorum longus (EDL), diaphragm, and heart, we did not observe any differences in total or phosphorylated GSK3 (Figure 1A-C). Nonetheless, GSK3 is a constitutively active enzyme that it is active even in the basal state[26]. Therefore, we sought to determine the effects of GSK3 inhibition in the D2 *mdx* mouse by first using the most clinically advanced GSK3 inhibitor, tideglusib. This drug belongs to the thiadiazolidindione (TDZD) family and is a non-ATP competitive GSK3 inhibitor that is currently in clinical trials for supranuclear palsy, Alzheimer's disease, and myotonic dystrophy type 1 (DM1)[21,22]. Mechanistically, tideglusib irreversibly binds to GSK3 and holds it in an inactive state[27], and although this is its primary mode of inhibition, tideglusib and other TDZD compounds can also reduce total GSK3 content and increase inhibitory serine phosphorylation[28,29]. In support of this, we found that tideglusib treatment significantly reduced GSK3β content in the EDL and in cardiac muscle when compared with vehicle controls (Figure 1D-E). We also found a significant increase Ser9 phosphorylation in the EDL, however, we did not find any changes in total or phosphorylated GSK3β content in the *mdx* diaphragm (Figure 1D-F).

After assessing muscle histopathology, we found that tideglusib treatment significantly reduced muscle necrosis while also lowering serum creatine kinase (CK) levels (Figure 1G-I). Tideglusib treatment also lowered muscle nitrocysteine and nitrotyrosine levels, which are markers of oxidative stress and necrosis (Figure S1). Not surprisingly, tideglusib treatment led to a

significant improvement in specific force generation at both sub-maximal and maximal stimulation frequencies (Figure 1J-K). Though the increase in specific force production cannot be attributed to an increase in muscle size, we did find that tideglusib treatment significantly increased the cross-sectional area (CSA) of all fibre types in the EDL (Figure 1L-M) - a result consistent with the known hypertrophic effect of GSK3 inhibition[9,30]. Moreover, and in agreement with the repressive action of GSK3 on the oxidative fibre type[9,10], tideglusib treatment significantly lowered the proportion of glycolytic type IIB fibres and led to trending increases in type I and IIA oxidative fibres (Figure 1N). These changes in muscle fibre type composition were associated with a reduction in whole-body respiratory exchange ratio (RER), suggestive of a shift towards fat oxidation (Figure S2). Finally, the increase in oxidative fibres was also associated with an increase in utrophin mRNA levels (Figure 1O), which is a dystrophin homolog that can provide compensatory membrane stability[31,32]. It is well-established that the expression of utrophin is controlled by NFAT signalling and is therefore tightly tied to the oxidative myogenic program[12,13,33]. Altogether, these data show that inhibition of GSK3 with tideglusib can lower necrosis and improve skeletal muscle contractility, partly by increasing muscle size but also by increasing the oxidative fibre type and utrophin content.

We then conducted cardiac morphological and functional analyses in WT, vehicle- and tideglusib treated D2 *mdx* mice via high frequency ultrasound. Table 1 shows that there were no differences in measured left ventricle (LV) mass relative to body mass. With high frequency ultrasound, we found signs of concentric remodelling with lowered left ventricle internal diameter (LVID) and increased relative wall thickness (RWT) in both *mdx* groups. Both end-diastolic volume (EDV) and end-systolic volume (ESV) were also lowered in vehicle treated and tideglusib treated D2 *mdx* mice compared with WT, however, this was only statistically significant for ESV.

There were no changes in stroke volume (SV) across groups, but % ejection fraction (%EF) was higher in vehicle treated and tideglusib treated D2 *mdx* mice compared with WT.

Pulsed wave (PW) doppler analysis of mitral valve inflow showed no differences in E wave velocity; however, A wave velocity was significantly slower in tideglusib treated D2 *mdx* mice vs. WT mice. In turn, calculating the E/A ratio showed that tideglusib treated D2 *mdx* mice had the highest E/A ratio, being significantly different from WT mice. Furthermore, E wave deceleration time (DT) was significantly lower in the vehicle treated D2 *mdx* mice compared with both WT and tideglusib treated D2 *mdx* mice, which is suggestive of increased LV stiffness[34]. Finally, when examining isovolumic contraction and relaxation times (IVCT and IVRT, respectively), we found that IVRT was significantly highest in the vehicle treated D2 *mdx* mice compared with both WT and tideglusib treated D2 *mdx* mice, whereas there were no differences detected across groups with IVCT. Overall, these results indicate that young (12-14 week old) D2 *mdx* mice show signs of concentric remodelling; and while systolic function is intact, and apparently even enhanced, diastolic dysfunction and reduced compliance can be observed in vehicle treated D2 *mdx* mice, but not in tideglusib treated D2 *mdx* mice. This apparent restoration of diastolic function and cardiac compliance with tideglusib treatment is likely due to a reduction in muscle oxidative stress (Figure S1), as we did not observe any changes in sarco(endo)plasmic reticulum Ca^{2+}-ATPase (SERCA) function or muscle fibrosis (Figure S3 and S4).

Lithium treatment improves muscle function in mdx mice subjected to voluntary wheel running

We next investigated the combined effects of exercise and GSK3 inhibition on muscle form and function in *mdx* mice. VWR was chosen as the mode of exercise given its low intensity and minimal stress added to the mouse. In line with minimizing stress on the animal during exercise

training, GSK3 inhibition was afforded with Li supplementation that was provided through drinking water rather than tideglusib via oral gavage. Li is a natural inhibitor of GSK3 and is most commonly used for the treatment of bipolar disorder; however, within a narrow therapeutic range of 0.5-1.0 mM serum Li concentration[35]. Here, we treated *mdx* mice with a low dose of lithium chloride (50 mg/kg/day via drinking water), which resulted in a serum Li concentration of 0.15 ± 0.05 mM (n = 9). Similar to our findings with tideglusib, Li supplementation improved specific force production in both soleus and EDL muscles (Figure 2A-B). In the soleus, WT mice produced significantly more force than *mdx* sedentary (*mdx*-SED) and *mdx*-VWR groups but no differences were found when comparing WT with *mdx*-VWRLi mice (Figure 2A). Furthermore, the soleus from the *mdx*-VWRLi group produced significantly more force when compared to the *mdx*-SED group at sub-maximal and maximal frequencies (Figure 2A). In the EDL, WT mice produced significantly more force compared with all *mdx* groups across submaximal and maximal frequencies (Figure 2B). However, the EDL from *mdx*-VWRLi mice produced significantly more force when compared with *mdx*-SED (160Hz), and *mdx*-VWR (20, 40, 80 and 160 Hz) groups (Figure 2B).

The improvements in contractile function observed in the *mdx*-VWRLi mice were associated with significant reductions in markers of oxidative stress (total nitrotyrosine and nitrocysteine) when compared with *mdx*-SED mice (Figure 2C-D). Histological staining also showed lowered muscle necrosis in the *mdx*-VWRLi mice (Figure 2E). Furthermore and similar to our tideglusib experiments, the *mdx*-VWRLi mice had the lowest RER compared with the *mdx*-SED mice, which is indicative of enhanced oxidative fiber expression (Figure S2). Given the fact that oxidative fibers are more insulin sensitive than their glycolytic counterparts[36] and that Li is a well-known insulin mimetic[35], we next examined the effects of VWR and Li on insulin sensitivity.

Insulin tolerance tests show that *mdx*-SED mice were insulin resistant compared with WT, *mdx*-VWR, and *mdx*-VWRLi mice (Figure 2E-F). Moreover, while VWR improved insulin tolerance in *mdx* mice, Li supplementation provided an additive effect (on top of exercise) whereby *mdx*-VWRLi mice had the lowest area-under-the-curve (AUC) compared with all *mdx* groups (Figure 2F). Notably, these metabolic and contractile benefits of Li were found with half the exercise volume. After measuring average daily distance travelled and total distance travelled, we found that the *mdx*-VWRLi group ran significantly less (-50%) than the *mdx*-VWR group when given access to a cagewheel (Figure 2G-H). Altogether, our results show that despite running less, Li supplementation along with VWR can significantly improve specific force production, reduce oxidative stress and necrosis, while also imparting metabolic benefits such as enhanced oxidative metabolism and insulin tolerance.

With respect to cardiac muscle, our experiments in *mdx*-VWRLi mice displayed similar results to our tideglusib treated mice with significantly prolonged DT compared with *mdx*-SED and *mdx*-VWR mice (Table 2). There were no differences between groups when assessing cardiac muscle morphology (i.e., internal diameter or relative wall thickness); however, *mdx*-VWR mice had significantly lowered %EF compared with *mdx*-SED mice, indicative of worsened cardiac contractile function in response to VWR. Importantly, this effect was not detected between *mdx*-SED and *mdx*-VWRLi mice (Table 2).

GSK3 inhibition improves cognitive function in mdx mice

GSK3 is a well-known target for various neurodegenerative diseases, and our results show that GSK3 content is elevated and less phosphorylated in the hippocampus from D2 *mdx* mice compared with WT mice (Figure 3A). This indicates that GSK3 is more active in the *mdx* brain.

Using a novel object recognition test (NORT) to investigate spatial memory, we found that while VWR appeared to increase total and novel investigation time, only the *mdx*-VWRLi mice had significantly greater total and novel investigation time compared with *mdx*-SED mice (Figure 3B-C). In fact, *mdx*-VWRLi mice also had greater novel investigation time compared with *mdx*-VWR mice. These effects were not due to any increase in distance travelled in the testing arena (Figure 3D), which is an important parameter to consider given that *mdx*-VWRLi mice had shown improvements in muscle health and function (Figure 2). In our recent work, we found that D2 *mdx* mice exhibited Alzheimer's like pathology with an alteration in brain biochemistry towards the production of β-amyloid (Aβ)[18]. BACE1 catalyzes the rate-limiting step in Aβ production; and GSK3 overactivation increases BACE1 expression and activation in the brain[20]. While we did not find any differences in BACE1 content in our previous work[18], in the present study, we found that Li supplementation significantly reduced BACE activity. Specifically, we found that the *mdx*-VWRLi mice had lower BACE activity compared with *mdx*-SED mice, which corresponds well with the improvements in cognitive function (Figure 3E). Similar to our experiments with Li, we also found that tideglusib treatment lowered BACE activity in the *mdx* hippocampus (Figure S6).

In addition to the production of Aβ, we also examined the level of vascular Aβ clearance. The pathological accumulation of Aβ oligomers in the brain can theoretically result from an overproduction and/or diminished clearance from the brain; and in sporadic Alzheimer's disease impaired Aβ clearance is known to be a key factor leading to Aβ accumulation[37]. Though the clearance of Aβ can occur through enzymatic degradation or non-enzymatically through transendothelial trafficking to circulating blood, the vascular pathway is the major route of removal from the brain[38]. Our results show that the *mdx*-VWRLi group had the highest levels of circulating Aβ, being significantly different from the *mdx*-SED group (Figure 3F). This indicates that the *mdx*-

VWRLi group had the greatest level of Aβ clearance, which when combined with significantly reduced BACE activity could contribute to improvements in cognitive function (Figure 3G).

Discussion

We investigated the potential therapeutic benefits of GSK3 inhibition on muscle and brain health in the D2 *mdx* mouse model. GSK3 has been shown to be a viable therapeutic target for other myopathic conditions such as myotonic dystrophy type 1 (DM1)[28], limb girdle muscular dystrophy[39], amyotrophic lateral scelerosis[40,41], and muscle disuse[11]. To our knowledge, no study has investigated the therapeutic potential of GSK3 inhibition for DMD, which would be important given that GSK3 inhibition not only enhances muscle health but is also an already established therapeutic strategy for various neurodegenerative diseases[42]. Here, our results show that treating D2 *mdx* mice with GSK3 inhibitors, alone or in combination with VWR, led to significant improvements in skeletal and cardiac muscle function, as well as spatial memory.

In *mdx* skeletal muscle, GSK3 inhibition can attenuate dystrophic pathology via several pathways and mechanisms including an enhancement in muscle size and quality, a reduction in oxidative stress, and a promotion in the oxidative fiber type program and utrophin expression. The increase in muscle size (i.e., increase in myofiber CSA) and improvement in muscle quality (i.e., lowered necrosis) observed with GSK3 inhibition can contribute to improvements in muscle force production and can be acquired through several pathways. First, GSK3 inhibition can enhance myogenic differentiation and fusion[30], which can aid in muscle regeneration in the face of constant degeneration. In addition, GSK3 inhibition can activate protein synthesis via the mTOR pathway[9]. Furthermore, GSK3 inhibition can attenuate oxidative stress, as previously seen in muscle and brain tissue[43,44], and this can also positively influence muscle size and quality. With respect to fiber

types, oxidative type I and IIA fibers are known to be more resistant to dystrophic pathology, partly because of their increased utrophin expression[13]. Utrophin can counteract dystrophic pathology in *mdx* mice with studies showing that an increase in its expression attenuates disease progression[12,45,46], whereas genetic deletion of utrophin accelerates disease in *mdx* mice[31,32]. Consistent with this, we found that tideglusib treatment promoted the oxidative fiber type leading to an increase in utrophin expression, an attenuation of dystrophic pathology, and an increase in specific force production. We also found that RER was significantly elevated in D2 *mdx* mice vs. WT mice, which is consistent with previous findings[47]. Furthermore, RER was effectively lowered with GSK3 inhibition, which is indicative of enhanced fat metabolism and can be attributed to a promotion of the oxidative fiber type[48]. These apparent benefits to metabolic health are clinically important especially when we acknowledge that DMD boys undergoing chronic glucocorticoid therapy are at increased risk for developing metabolic disorders such as obesity and type 2 diabetes that ultimately further the risk of cardiovascular disease and mortality[49-51]. In this context, GSK3 inhibition has already been shown to attenuate obesity and diabetes in other mouse models[52-54], and here we found that Li supplementation (a known insulin mimetic) not only improved muscle force but also enhanced insulin sensitivity. Thus, GSK3 inhibition can not only improve skeletal muscle form and function but may also diminish the risk of metabolic syndrome observed with glucocorticoid treatment.

Given that most patients will succumb to cardiorespiratory failure, we also investigated the effects of GSK3 inhibition on cardiac muscle morphology and contractility. In terms of morphology, we found signs of concentric hypertrophy in D2 *mdx* mice that were not resolved with any form of GSK3 inhibition. When compared to WT, we did not find any impairments in systolic function as %EF was not lower in D2 *mdx* mice. This is likely due to the age that we chose

(10-14 weeks) since impaired systolic function only manifests in older D2 *mdx* mice (~28 weeks)[55]. In fact, we found the opposite, where D2 *mdx* mice (vehicle and tideglusib treated) had greater EF% compared with WT controls (Table 1). This apparent increase in systolic function is consistent with a previous study using 21-week-old D2 *mdx* mice[46]. However, we did find that %EF was significantly reduced in D2 *mdx* mice that were given access to a cagewheel, suggesting that VWR may negatively impact cardiac contractile function in D2 *mdx* mice. This result is inconsistent with a previous study, which showed that VWR had no negative impact on cardiac contractile function in aged (7-month old) *mdx* mice[24]. While we do not know the exact cause of this discrepancy, we note that this previous study used C57BL/10 *mdx* mice and our present study is the first to show the effects of VWR in D2 *mdx* mice, which highlights a potential strain difference in response to exercise. That is, we speculate that the increased level of work and contractile stress observed with cagewheel running combined with the higher degree of disease severity in D2 *mdx* mice is likely what led to the reduction in %EF when compared to *mdx*-SED mice (Table 2). Importantly, the reduction in %EF was not found in *mdx*-VWRLi mice, which suggests that Li supplementation along with exercise training can protect against cardiac dysfunction in the *mdx* mouse. Indeed, this result may also be due to the fact that *mdx*-VWRLi mice ran half the total distance compared with *mdx*-VWR mice.

In addition to our measures of systolic function, our study is the first to show that young D2 *mdx* mice present with diastolic dysfunction that manifests as impaired relaxation (prolonged IVRT) and lowered compliance (shortened DT) when compared with WT mice (Table 1). Tideglusib treatment rescued IVRT in D2 *mdx* mice suggesting that GSK3 inhibition can improve muscle relaxation. However, IVRT in the *mdx*-VWRLi mice was not different from *mdx*-SED or *mdx*-VWR mice, which indicates that Li supplementation in the face of VWR could not improve

muscle relaxation. This may be due to the presence of exercise, though we cannot discount differences in drug response. Nonetheless, our data suggests that GSK3 inhibition alone (i.e., without exercise) can improve muscle relaxation. DT is the E wave deceleration time, and is the time taken for LV and left atrial pressures to equalize during LV diastolic filling. It has been used as a valid and non-invasive marker of LV stiffness and compliance in humans[34]. In a stiffened ventricle, such as that shown here in vehicle-treated D2 *mdx* hearts, DT will be shortened; however, this was lengthened and rescued with tideglusib treatment. Similarly, we found that *mdx*-VWRLi mice had significantly longer DT when compared with both *mdx*-SED and *mdx*-VWR mice (Table 2). Thus, our results indicate that GSK3 inhibition alone or with exercise can enhance compliance in D2 *mdx* hearts. These apparent improvements in diastolic function with GSK3 inhibition are attributed to a reduction in oxidative stress (Figure S1 and Figure 2) as we did not see any improvements in SERCA function (Figure S4) or reductions in myocardial fibrosis (Figure S5). Elevated oxidative stress can lead to diastolic dysfunction and lowered compliance, purportedly through negative alterations in titin which increase passive stiffness in the cardiomyocyte[56]; however, we are limited in that we have not examined the oxidant status of titin.

Finally, we investigated the effects of GSK3 inhibition on cognitive function and brain biochemistry in the *mdx* mouse. In contrast with muscle, hippocampal total GSK3 levels were higher while phosphorylated GSK3 levels were lower in *mdx* mice vs. WT mice. Thus, GSK3 is overactive in the *mdx* brain and may be contributing to the cognitive decline that we and others have found in the *mdx* mouse[18,57-59]. In support of this, *mdx*-VWRLi mice showed improvements in spatial memory with enhanced novel object recognition when compared with *mdx*-SED mice. VWR without Li also appeared to improve novel object recognition, which is consistent with the known effect of VWR and exercise on improving spatial memory; however, this effect did not

reach statistical significance. Furthermore, we found that *mdx*-VWRLi mice had greater novel object recognition compared with *mdx*-VWR mice, suggesting that Li supplementation had an additive effect, which is impressive given that the *mdx*-VWRLi mice ran significantly less. Thus, we attribute the improvements in spatial memory in the *mdx*-VWRLi mice largely to Li supplementation, which is consistent with the neuroprotective effects of Li[35,60-62].

Mechanistically, we explored the effects of Li supplementation on both Aβ production via BACE activity, and vascular clearance by measuring serum Aβ levels. We specifically focused on Aβ production/clearance as we have shown that D2 *mdx* mice present with Alzheimer's-like pathology and a shift towards amyloidogenesis[18]. Consistent with previous literature showing that Li treatment can reduce BACE activity and β-amyloid production to improve cognitive function in various mouse models[63,64], we found that *mdx*-VWRLi mice had significantly lower BACE activity compared with *mdx*-SED mice. We observed a similar result with tideglusib treatment (Figure S6); and thus our results are consistent with GSK3 regulating BACE activity in the brain[20]; however, we are limited in that we did not assess object recognition in these mice.

Aside from the production of Aβ, we also examined the potential for its vascular clearance, as this is often impaired in Alzheimer's disease[37]. Our results show that *mdx*-VWRLi mice had the greatest circulating levels of Aβ when compared with *mdx*-SED mice, which is indicative of enhanced clearance from the brain. The clearance of Aβ from the brain can occur enzymatically through enzymes such as the insulin degrading enzyme (IDE), as well as non-enzymatically by transport across the blood brain barrier and into circulation[38]. Insulin resistance and hyperinsulinemia can negatively affect both enzymatic and non-enzymatic clearance of Aβ. First, hyperinsulinemia can sequester IDE, which is not only responsible for degrading insulin, but also Aβ, ultimately allowing for Aβ oligomers to accumulate[65,66]. Secondly, hyperinsulinemia, insulin

resistance, and the ensuing hyperglycemia can negatively affect vascular clearance by causing blood brain barrier dysfunction and actually promoting the influx of Aβ back into the brain[38,67]. Indeed, Aβ can be transported bi-directionally through the blood brain barrier. The balance between clearance and re-uptake is largely controlled by the receptor of advanced glycation end products (RAGE), which facilitates the uptake of Aβ into the brain; and low-density lipoprotein receptor related protein 1 (LRP1), which facilitates vascular clearance[68]. Advanced glycation end products (AGEs) are protein or lipids that become glycated as a result of exposure to elevated glucose. Given that we and others have shown that *mdx* mice exhibit drastic impairments in glucose regulation with signs of insulin resistance, it is likely that *mdx* mice have greater RAGE activation and thus uptake of Aβ into the brain. However, since *mdx*-VWRLi mice had the greatest improvements in insulin sensitivity, we suspect that these improvements in glucose regulation contributed to the improvements in vascular Aβ clearance. Furthermore, LRP1 is sensitive to oxidative stress, as oxidation of LRP1 can impair vascular clearance leading to Aβ accumulation in the brain[38]. As with our results in cardiac and skeletal muscle, we find that markers of oxidative stress are lowered in the *mdx* hippocampus after treating with GSK3 inhibitors (Figure S7). In all, our results show that GSK3 inhibition can favourably alter the balance between Aβ production and clearance to ultimately improve cognitive function in *mdx* mice.

We were strategic in the GSK3 inhibitors chosen for this study. Tideglusib is the most clinically advanced GSK3 inhibitor that is currently being used in Phase II clinical trials for Alzheimer's disease, progressive supranuclear palsy, myotonic dystrophy, and autism spectrum disorders[21,22]. This is important as it could lead to a more rapid clinical integration for DMD. Furthermore, the dose that we chose to study was chosen to reflect a 600 mg dose for a 60 kg individual, which is in line with clinical trials for myotonic dystrophy[69]. Li is an already FDA-

approved drug used in the treatment of bipolar disorder. Though Li toxicity has been observed in the clinical setting, these adverse events have been associated with long term therapy with relatively higher doses (above serum Li of 1.0 mM)[35]. In the present study, we used a dose below the clinically used window of 0.5 mM – 1.0 mM serum Li concentration, which was still able to produce significant benefits on skeletal muscle specific force production, cardiac muscle diastolic and systolic function, and metabolic and cognitive health in *mdx* mice.

We chose to combine Li supplementation with VWR to determine whether the improvements in VWR previously observed in *mdx* mice[25] could be amplified with GSK3 inhibition. VWR is considered as a low intensity and minimal stress model of exercise in mice, and we did not want to add any stress with the oral gavage of tideglusib. VWR has been shown to attenuate muscle pathology in *mdx* mice and improve muscle force production partly by activating calcineurin[24,25]. Calcineurin is a Ca^{2+}-dependent phosphatase that dephosphorylates NFAT and is best known for its role in promoting the oxidative phenotype[13,70-73] that can be used to attenuate dystrophic pathology in *mdx* mice[12,15,74,75]. We and others have shown that GSK3 counteracts calcineurin signalling by re-phosphorylating NFAT[10,76,77], and thus the combined effects of calcineurin activation with exercise plus GSK3 inhibition could lead to additive benefits on skeletal muscle function. Consistent with this, we found that skeletal muscles from the *mdx*-VWRLi mice produced the most force compared with *mdx*-SED and *mdx*-VWR mice, and these mice also had the lowest RER – indicative of enhanced oxidative metabolism. They were also the most-insulin sensitive, and all of these benefits were found despite the *mdx*-VWRLi mice running significantly less than *mdx*-VWR mice. While we do not have an explanation for these differences in exercise volume, we have also found that muscle-specific GSK3 knockdown mice run significantly less than their flox controls; however, despite these differences, these mice were able

to attain the same improvement in insulin tolerance when compared with sedentary controls (Figure S8). This reveals a clinically important aspect of GSK3 inhibition in combination with exercise. Given that DMD primarily affects muscle, the role of exercise in disease management has been controversial[78]. Furthermore, those that are more affected by DMD may be unable to exercise adequately. Thus, our results showing that GSK3 inhibition with small amounts of VWR or aerobic exercise can impart benefits on muscle, brain, and metabolic health can be clinically impactful.

In summary, we found that treating D2 *mdx* mice with GSK3 inhibitors, tideglusib or Li, improved skeletal muscle and cardiac muscle contractility along with providing benefits to metabolic health (oxidative metabolism and glucose regulation) and cognitive function. The benefits imparted by GSK3 inhibition are multifactorial with a shift towards the oxidative fiber type, an increase in muscle size, a reduction in oxidative stress, and brain BACE activity. Altogether, these results have the potential to dramatically improve the quality of life of those living with DMD and should be tested in the clinical setting with either tidgelusib or low dose Li therapy.

Limitations of the study

We acknowledge several limitations to our study. First, we only used young D2 *mdx* mice. While this age was chosen to reflect the age of the DMD population as 10-14 weeks is equivalent to 15-20 human years, dystrophic pathology in D2 *mdx* mice, like that in humans, is progressive[55,79]. Thus, it would be important to determine the effects of GSK3 inhibition in older D2 *mdx* mice where skeletal muscle weakness, cardiac muscle function, and spatial memory would be worsened. Furthermore, it would be important to examine the effects of long-term GSK3 inhibition, specifically determining whether it can slow the progression of dystrinopathy in *mdx*

mice. Our study is also limited in that we only tested one mouse model of DMD; and though the D2 *mdx* mouse model is more severe than the C57BL/10 future studies could examine the effects of GSK3 inhibition on the mdx/utrophin double knockout mice. With respect to cognitive function, we only used the NORT to examine cognitive function, and there are a battery of other tests that could be used. We also restricted our focus to Alzheimer's disease pathology based on our previous work; and whether this holds true for human DMD patients remain unknown. Nonetheless, and outside of Alzheimer's disease, GSK3 inhibition has been shown to provide neuroprotection against several different diseases through several other pathways[80]. Thus, the inhibition of GSK3 could still potentially improve cognitive function in DMD patients, even if not tied to β-amyloid production, and this should be tested in the clinical setting. Despite these limitations, our study is the first to reveal a potential universal treatment strategy for DMD focusing on both muscle and brain health to ultimately enhance quality of life.

Acknowledgements

This work was supported by an unrestricted Brock University Grant and a Canada Research Chair (Tier 2) award to VAF. SIH was supported by a NSERC Doctoral Vanier Award, JLB was supported by a CIHR CGS-D award, and BH was supported by an Ontario Graduate Scholarship. We thank Tonya Coulthard (Scintica Instruments) for her help with high frequency ultrasound analysis. We thank the animal care staff at Brock University for their assistance with animal care and handling.

Author contributions

BMM - Concept design, writing and drafting the manuscript, figure creation, data collection, data interpretation, particularly on skeletal muscle function.
EC - Concept design, writing and drafting the manuscript, figure creation, data collection, data interpretation, particularly on cognitive function and brain biochemistry.
SIH – Concept design, writing and drafting the manuscript, figure creation, data collection, data interpretation, particularly on cardiac muscle function.
BH – Data collection, data interpretation, reviewing and revising the manuscript
JLB – Data collection, data interpretation, reviewing and revising the manuscript
MG – Data collection, data interpretation, reviewing and revising the manuscript
KCW – Data collection, data interpretation, reviewing and revising the manuscript
CJFW – Data collection, data interpretation, reviewing and revising the manuscript
BJB – Data collection, data interpretation, reviewing and revising the manuscript
ECO – Data collection, data interpretation, reviewing and revising the manuscript
AM – Data collection, data interpretation, reviewing and revising the manuscript
SS – Data collection, data interpretation, reviewing and revising the manuscript
RWB – Data collection, data interpretation, reviewing and revising the manuscript
LW – Data collection, data interpretation, reviewing and revising the manuscript
REGC – Data collection, data interpretation, reviewing and revising the manuscript
SB - Provision of reagents and resources, reviewing and revising the manuscript
RV – Provision of reagents and resources, reviewing and revising the manuscript
BDR – Provision of reagents and resources, reviewing and revising the manuscript
JAS – Provision of reagents and resources, reviewing and revising the manuscript
AJM – Provision of reagents and resources, reviewing and revising the manuscript
REKM – Concept design, supervision, provision of reagents and resources, writing and drafting the manuscript
VAF – Concept design, supervision, provision of reagents and resources, acquiring funding, writing and drafting the manuscript

Competing interests

The authors declare that there are no conflicts of interests to report.

FIGURE LEGENDS

Figure 1. Tideglusib treatment reduces muscle necrosis and improves skeletal muscle contractility (see Figure S1 and S2).

(A-C) Western blot analysis of total and serine (Ser) 9 phosphorylated GSK3β in EDL, diaphragm, and cardiac muscle homogenates from D2 WT and *mdx* mice. Analyzed with a Student's t-test (per muscle) (n = 6-9 per group).

(D-F) Western blot analysis of total and serine (Ser) 9 phosphorylated GSK3β in EDL, diaphragm, and cardiac muscle homogenates from vehicle and tideglusib treated D2 *mdx* mice. Analyzed with a Student's t-test (per muscle) (n = 5-6 per group).

(G-H) H&E staining of EDL muscles from vehicle and tideglusib treated D2 *mdx* mice showing significant reductions in necrotic area (areas occupied by fibrosis and immune cell infiltration). Analyzed with a Student's t-test, (n = 4 per group). Scale bars are set to 200 μM.

(I) Serum creatine kinase (CK) levels are significantly elevated in vehicle treated *mdx* mice compared with tideglusib treated *mdx* mice. Analyzed with a Student's t-test, (n = 11-12 per group).

(J) Representative witch and tetanic (150 Hz) force tracings from EDL muscles from vehicle and tideglusib treated D2 *mdx* mice.

(K) Force frequency curve analysis shows that tideglusib treatment enhances EDL specific force generation. Analyzed with a two-way ANOVA where a significant interaction between frequency and tideglusib ($p < 0.0001$) was detected (n = 10-11 per group). An uncorrected Fisher's LSD test was used at the individual frequencies.

(L-N) Immunofluorescent fiber type staining show an increase in myofiber cross-sectional area (CSA) and a significant reduction in type IIb fibers. Analyzed with a Student's t-test (per muscle) (n = 4 per group).

(O) Utrophin *mRNA* analysis in plantaris muscles from vehicle treated and tideglusib treated D2 *mdx* mice. Analyzed with a Student's t-test (n = 7-10 per group).

All values are mean ± SEM. *$p<0.05$, **$p<0.01$.

Figure 2. Lithium treatment improves muscle function in *mdx* mice subjected to voluntary wheel running (see Figure S2).

(A) Force frequency curve analysis in soleus muscles from WT, *mdx*-SED, *mdx*-VWR, *mdx*-VWRLi mice. Data were analyzed with a two-way ANOVA where a significant interaction between frequency and tideglusib ($p < 0.0001$) was detected (n = 8-9 per group). An uncorrected Fisher's LSD test was used at the individual frequencies.

(B) Force frequency curve analysis in EDL muscles from WT, *mdx*-SED, *mdx*-VWR, *mdx*-VWRLi mice. Data were analyzed with a two-way ANOVA where a significant interaction between frequency and tideglusib ($p = 0.0002$) was detected (n = 8-9 per group). An uncorrected Fisher's LSD test was used at the individual frequencies.

(C-D) Markers of oxidative stress, protein nitrocysteine and protein nitrotyrosine levels were measured via western blot analysis in EDL and soleus muscles from *mdx*-SED, *mdx*-VWR, and *mdx*-VWRLi mice. Data were analyed with a two-way ANOVA where a main effect of condition was detected ($p = 0.01$ for nitrocysteine, $p = 0.04$ for nitrotyrosine), and a Tukey's post-hoc test then applied (n = 5-11 per group).

(E) H&E staining showing lowered muscle necrosis in *mdx*-VWRLi muscles with less signs of fibrosis and immune cell infiltration. Scale bars are set to 200 μM.

(F-G) Insulin tolerance tests and corresponding area-under-the-curve (AUC) analysis in WT, *mdx*-SED, *mdx*-VWR, *mdx*-VWRLi mice. Glucose traces were analyzed using a two-way ANOVA with a Tukey's post-hoc test (n = 11 per group). AUC were analyzed using a one-way ANOVA with a Tukey's post-hoc test (n = 11 per group).

(H-I) Daily cage wheel distance and total distance travelled from *mdx*-VWR and *mdx*-VWRLi mice. Data were analyzed using a Student's t-test, (n = 11 per group).

All values are mean ± SEM. The number of each symbol denotes level of statistical significance. For example, *$p<0.05$, **$p<0.01$, ***$p<0.001$, ****$p<0.0001$.

Figure 3. GSK3 inhibition improves cognitive function in mdx mice
(A) Total and Ser9 phosphorylated GSK3β in WT and *mdx* hippocampus. Data analyzed with a Student's t-test (n = 4 per group).
(B-D) Novel object recognition tests in *mdx*-SED, *mdx*-VWR, and *mdx*-VWRLi mice show that *mdx*-VWRLi mice have longer total investigation and novel object recognition time without now differences in total difference covered in the arena. Data analyzed with a one-way ANOVA and a Tukey's post-hoc test (n = 8-9 per group).
(E) Enzymatic BACE activity in hippocampal regions obtained from *mdx*-SED, *mdx*-VWR, and *mdx*-VWRLi mice. Data analyzed with a one-way ANOVA and a Tukey's post-hoc test (n = 4-5 per group).
(F) Serum $A\beta_{42}$ levels in *mdx*-SED, *mdx*-VWR, and *mdx*-VWRLi mice. Data analyzed with a one-way ANOVA and a Tukey's post-hoc test (n = 5-6 per group).
(G) Proposed pathway demonstrating the benefits of GSK3 inhibition on Aβ production/clearance and cognitive function.

Table 1. High-frequency ultrasound analysis of cardiac muscle morphology and function in in age-matched wild-type (WT), vehicle and tideglusib treated *mdx* mice (see Figure S3 and S4).

	WT	*mdx*-vehicle	*mdx*-tideglusib
LV:body mass	3.81 ± 0.12	3.81 ± 0.15	4.0 ± 0.14
LVID;d (mm)	3.59 ± 0.12	3.23 ± 0.12	3.31 ± 0.13
LVID;s (mm)	2.33 ± 0.10	1.81 ± 0.10**	1.82 ± 0.13**
RWT;d	0.58 ± 0.03	0.73 ± 0.04*	0.71 ± 0.04†
RWT;s	1.23 ± 0.08	1.90 ± 0.16**	1.88 ± 0.16**
EDV (ml)	55.1 ± 4.1	42.7 ± 4.1†	42.0 ± 2.9†
ESV (ml)	19.3 ± 1.9	10.43 ± 1.63**	10.9 ± 2.0**
SV (ml)	35.8 ± 2.8	32.3 ± 2.5	34.5 ± 2.8
EF (%)	65.0 ± 2.2	76.3 ± 1.6**	77.0 ± 2.6**
E velocity (mm/s)	672.4 ± 30.2	615.1 ± 30.0	616.5 ± 37.9
A velocity (mm/s)	508.8 ± 26.1	433.6 ± 24.5	404.9 ± 30.6*
E/A ratio	1.3 ± 0.1	1.4 ± 0.1	1.5 ± 0.1*
DT (ms)	35.3 ± 1.2	26.3 ± 2.6*	33.9 ± 1.9$^{\#}$
IVCT (ms)	9.4 ± 1.0	9.6 ± 0.6	10.2 ± 0.8
IVRT (ms)	14.4 ± 0.5	17.4 ± 0.4***	14.9 ± 0.7$^{\#\#}$

LV:body mass, measured LV:body mass ratio; LVID;d, left ventricle internal diameter diastole; LVID;s, left ventricle internal diameter systole; RWT;d, relative wall thickness diastole; RWT;s, relative wall thickness systole; EDV, end-diastolic volume; ESV, end-systolic volume; SV, stroke volume, EF; ejection fraction; DT, deceleration time; IVCT, isovolumic contraction time; IVRT, isovolumic relaxation time. A one-way ANOVA with a Tukey's post-hoc test was used; vs. WT, $^{\dagger}p < 0.10$, $*p < 0.05$, $**p < 0.01$; vs. *mdx*-vehicle, $^{\#}p < 0.05$, $^{\#\#}p < 0.01$; using a One-way ANOVA with a Tukey's post-hoc test, (n=10-12 per group except for LV:body mass, n = 6 per group).

Table 2. High-frequency ultrasound analysis of cardiac muscle morphology and function in age-matched *mdx* -SED, *mdx*-VWR, and *mdx*-VWRLi mice.

	***mdx*-SED**	***mdx*-VWR**	***mdx*-VWRLi**
LVID;d (mm)	3.63 ± 0.14	3.82 ± 0.10	3.9 ± 0.10
LVID;s (mm)	2.37 ± 0.22	2.84 ± 0.15	2.78 ± 0.17
RWT;d	0.70 ± 0.08	0.68 ± 0.06	0.69 ± 0.05
RWT;s	1.38 ± 0.21	1.02 ± 0.07	1.17 ± 0.18
EDV (µL)	56.7 ± 5.1	63.8 ± 4.1	69.6 ± 3.3
ESV (µL)	22.6 ± 5.1	31.5 ± 3.8	30.1 ± 4.0
SV (µL)	34.2 ± 2.2	32.4 ± 3.0	39.5 ± 2.3
EF (%)	67.8 ± 4.2	51.2 ± 4.4*	57.3 ± 4.5
E velocity (mm/s)	364.1 ± 28.8	403.4 ± 38.4	399.1 ± 36.9
A velocity (mm/s)	270.0 ± 24.5	283.1 ± 27.4	285.9 ± 15.7
E/A ratio	1.40 ± 0.09	1.45 ± 0.07	1.39 ± 0.08
DT (ms)	30.6 ± 2.5$^{\#\#}$	30.6 ± 2.4$^{\#\#}$	44.3 ± 3.4
IVCT (ms)	15.0 ± 1.1	15.0 ± 1.2	14.7 ± 0.3
IVRT (ms)	25.9 ± 0.5	27.1 ± 1.4	28.8 ± 0.7

LVID;d, left ventricle internal diameter diastole; LVID;s, left ventricle internal diameter systole; RWT;d, relative wall thickness diastole; RWT;s, relative wall thickness systole; EDV, end-diastolic volume; ESV, end-systolic volume; SV, stroke volume, EF; ejection fraction; DT, deceleration time; IVCT, isovolumic contraction time; IVRT, isovolumic relaxation time. A one-way ANOVA with a Tukey's post-hoc test was used; * vs. *mdx*-SED $p<0.05$, $^{\#\#}$vs. *mdx*-VWRLi, $p < 0.01$. All values are mean ± SEM (n = 7-11).

STAR METHODS

RESOURCE AVAILABILITY

Lead contact

Further information and requests for resources and reagents should be directed to and will be fulfilled by the lead contact, Val A. Fajardo (vfajardo@brocku.ca).

Materials availability

This study did not generate new unique reagents.

Data and code availability

All data are included in the published article or are available from the lead contact upon reasonable request. This paper does not report original code.

EXPERIMENTAL MODELS AND SUBJECT DETAILS

Mice and Design

DBA/2J (D2)-*mdx* (stock #001801) and D2 WT (stock #000671) were ordered from Jackson Laboratories at 5-6 weeks of age. Muscle-specific GSK3 KD mice were generated in our lab using cryorecovered GSK3 α and β floxed mice[81]. All mice were housed in Brock University's Animal Facility, in an environmentally controlled room with a standard 12:12 hour light-dark cycle and allowed access to food and water *ad libitum*.

Tideglusib treatment

D2 *mdx* mice were treated with tideglusib at a dose of 10mg/kg/day via oral gavage, whereas a separate vehicle group of D2 *mdx* mice were given 26% peg400, 15% Chremaphor EL

and water [28] for 5 days per week. A separate group of WT mice were also housed simultaneously to serve as a healthy reference control. D2 *mdx* mice were treated for a period of 2-4 weeks to allow for a variety of *in vivo* measures to be conducted. A subset of D2 *mdx* (vehicle and tideglusib) mice were euthanized after 2 weeks to examine GSK3 activation, fiber type composition and necrosis via histological staining (n=5-6 per group). The remaining mice were treated for an additional two weeks to conduct several *in vivo* measures and additional biochemical (SERCA function and western blotting) and histological measures (cardiac histology) (n=10-12 per group).

Voluntary wheel running and Li supplementation

D2 *mdx* mice were randomly divided into 3 groups: 1) *mdx*-SED, 2) *mdx*-VWR, and 3) *mdx*-VWRLi (n = 11 per group). The VWR groups were provided with a cage wheel for 6 weeks and all mice were housed in the Techniplast DVC80 with GYM500 software to track cage wheel distance travelled 24/7. The Li-fed *mdx* mice were provided lithium chloride (50 mg/kg/day) in their drinking water with 2 water changes per week for the entire duration of the study.

METHOD DETAILS

RER analysis

Mice were housed in the Promethion Metabolic Screening System for a period of 48 hours to track fuel utilization. The cages are connected to a flow regulator and O_2 and CO_2 gas analyzers which measure the volume of carbon dioxide produced (VCO_2) and the volume of oxygen consumed (VO_2). Respiratory exchange ratio (RER) was calculated as VCO_2 divided by VO_2.

Insulin tolerance test

Insulin tolerance testing was performed as previously described[81]. Briefly, concentrations of blood glucose were determined by sampling blood from the tail vein at 0, 15, 30, 60, and 120 min following the IP insulin injection (0.5 U/kg) with the use of a hand-held glucometer (Freestyle Lite; Abbott). Plots of the average changes in plasma glucose over time were made for each group, and the average total area under the curve was calculated. Area under the curve is presented in mmol/l × time, and baseline values are set to X = 0.

High frequency ultrasound

Mice were subjected to high frequency ultrasound analysis using a Prospect T1 high frequency ultrasound (S-Sharp, Taiwan). Short axis M-mode imaging was used to calculate systolic function, including the LVID, RWT, EDV, ESV, SV, %EF. PW doppler of the mitral valve inflow, from an apical 4-chamber view, was used to assess diastolic function, specifically measuring E velocity, A velocity, deceleration time, IVRT and IVCT. Measurements were taken at a maintained heart rate of 400-550 bpm.

Novel object recognition test

Novel object recognition tests were performed as previously described[18] but modified so that data analysis was automated with MatLab computer software (MathWorks Inc.). The mice were habituated to the arena the day prior to testing where they could explore freely. Following the habituation, the mice were placed in the arenas with two identical objects in the bottom corners and were left to explore for 10-minutes. The mice were then returned to their home cages for a 60-

minute intertrial retention delay. Next, the mice returned to the arena where one of the familiar objects was replaced by a novel object and they were given 10-minutes to explore.

Sample and tissue collection

All mice were euthanized via exsanguination under general anesthetic (vaporized isoflurane) and their tissues and blood were collected. Blood was spun at 5000 x g for 8 minutes (4˚C) and serum was collected and stored at -80˚C. Extensor digitorum longus (EDL), soleus, plantaris, diaphragm, gastrocnemius, quadriceps, cardiac muscles, and hippocampal brain regions were isolated and stored at -80˚C for further analysis.

Isolated muscle contractility

Soleus and EDL muscles were carefully dissected and mounted onto an Aurora Scientific contractile apparatus (model 305B&701B) to assess muscle force production and fatigue as previously described[10]. Muscles were subjected to a force-frequency protocol (1–160 Hz). For data analyses, peak isometric force amplitude (mN) was determined across the range of stimulation frequencies. Peak isometric force was then normalized to muscle cross-sectional area (CSA), which was calculated using the following formula: $CSA = m/l*d*(L_f/L_o)$, where m, muscle mass (mg); l, muscle length (mm); d, mammalian skeletal muscle density (1.06 mg/mm^3)[82]. Lf/Lo is the fiber length-to-muscle length ratio (0.44 for the EDL and 0.71 for the soleus)[83].

Serum CK, Li, and $A\beta_{42}$ analysis

Serum creatine kinase (CK) activity was measured with a M2 Molecular Device plate reader and a commercially available assay (Cat. #C7522, Pointe Scientific Inc., Canton, MI, USA) fitted onto a 96-well plate and calibrated with a standard curve of purified creatine kinase (Sigma,

Oakville, ON, Canada, Cat. 10127566001). Serum Li analysis in the *mdx*-VWRLi mice were measured using the commercially available kit (ab235613, Abcam). Serum $A\beta_{42}$ content was measured using the commercially available kit (KMB3441, Life Technologies).

Immunofluorescent fiber typing

Fiber typing was accomplished through immunofluorescent staining of myosin heavy chain (MHC) isoforms in 10 μm sections of the EDL and soleus muscles as previously described[84]. Slides were imaged using a BioTek Cytation 5 Multimode Plate Reader at 10x magnification using auto-exposure settings for three filters: DAPI, GFP, and Texas Red. Images were then stitched, processed and saved using the Gen5 image processing functions, and then analyzed using ImageJ (NIH) software to estimate fiber type composition and CSA.

Histological assessment

For EDL and soleus muscles, necrosis (was measured using Hematoxylin and Eosin (H&E) staining of EDL muscle samples. All slides were imaged using a BioTek Cytation 5 Multimode Plate Reader. All images were acquired using 10x magnification using auto-exposure settings for the Colour Brightfield setting. Images were then saved and then analyzed using ImageJ (NIH) software to estimate necrotic area. This was done by calculating the total surface area of the muscle, then calculating the sum of the area of all necrosis (areas occupied by collagen and immune cell infiltration) within the sample. This total necrosis was then divided by the total area of the sample.

For cardiac histology, hearts were isolated and fixed in 10% formalin for 72hrs then transferred to 70% (v/v) ethanol until being embedded in paraffin wax (n = 5 per group). Slices 10 μm in size were affixed to vectabond-treated slides and stained with Gamori trichrome stain with

muscle tissues stained red, nuclei stained black and fibrotic tissue stained blue. Images were taken at 20x magnification at the apex, base and mid-region of the left ventricle of the heart (4-6 images per area). Images were analyzed using ImageJ software (US National Institutes of Health) to identify % fibrosis by measuring total blue area (fibrotic tissue) divided by total red area (muscle tissue) x 100%.

Western blotting

Western blotting was done to assess protein levels of GSK3β, Ser9 phosphorylated GSK3β, and total protein nitration (nitrotyrosine) and nitrosylation (nitrocysteine). Standard SDS-PAGE was performed with BioRad 7-12% TGX gels (4561086; BioRad, Hercules, CA, USA) and polyvinylidine difluoride (PVDF) membranes were used for all proteins (BioRad). All protein blots were blocked with Everyblot buffer (#12010020, BioRad) for 10 min at room temperature and incubated with primary and corresponding secondary antibodies (Supplementary Table 1) prior to imaging with a BioRad ChemiDoc Imager with Immobilon ECL Ultra Western HRP Substrate (WBKLS0500, Sigma-Aldrich). Images were analyzed using BioRad ImageLab software (BioRad) and were normalized to total protein analyzed on a Ponceau stain or GAPDH.

mRNA analysis

mRNA analyses for utrophin (forward, GGGGAAGATGTGAGAGATTT; reverse, GTGTGGTGAGGAGATACGAT) was accomplished by homogenizing plantaris samples with 1mL of TRIzol. A commercially available Qiagen RNeasy kit (Quiagen, Hilden, Germany, ID #74104) and a DNase Max kit (Quiagen, Hilden, Germany, D #15200-50) was then used to isolate RNA. This was then quantified using a NanoVue Plus spectrophotometer (Biochrom Ltd., Cambridge, UK), followed by the use of EcoDry RNA to cDNA (Takara Bio Inc., Kusatsu, Shiga,

Japan, ID #639547) reaction tubes and a SimpliAmp Thermal Cylinder (ThermoFisher, MA, USA, ID #A24811) to facilitate the generation of cDNA. Diluted cDNA was then analyzed using a qPCR reaction 96-well plate and the StepOnePlus Real-Time PCR System (ThermoFisher, MA, USA, ID #4376600). Threshold cycle (Ct) values were recorded, and data were analyzed using the ΔΔCt method and reported as a foldchange (2ΔCt), using expression of the Gapdh housekeeping gene as a reference (forward, CGGTGCTGAGTATGTCGTGGAGTC; reverse, GGGGCTAAGCAGTTGGTGGTG; IDT).

SERCA function

SERCA function was assessed in diaphragm and cardiac muscle homogenates using an oxalate-supported Ca^{2+} uptake fluorimetric assay and an ionophore (A23187, Sigma Aldrich)-supported spectrophotometric SERCA activity assay, both fitted onto a 96-well plate using an M2 MultiMode plate reader (Molecular Devices) as previously described[85,86]. For both Ca^{2+} uptake and SERCA activity, rates were normalized to total protein obtained from a BCA assay.

Dichlorofluorescein (DCF) assay

DCF assays were performed in hippocampal regions from the D2 WT and *mdx* brain to assess total reactive oxygen species (ROS) levels as briefly described [87]. Tissue homogenates (25 ul) were incubated with 5 μM 2′,7′-Dichlorofluorescin diacetate (D6883, Sigma) for 10 minutes at 37°C. Fluorescence was measured using an M2 Multimode Plate reader (emission: 490 nm and excitation: 525 nm) and was normalized to total protein obtained from a BCA assay.

Ethics statement

All animal procedures were approved by the Brock University Animal Care and Utilization Committee (file #17-06-03, 20-07-01, and 22-04-01) and were carried out in accordance with the Canadian Council on Animal Care guidelines.

QUANTIFICATION AND STATISTICAL ANALYSIS

Statistical analysis

Statistical comparisons were made using a Student's t-test, a one-way or two-way ANOVA with a Tukey's or Fisher's LSD post-hoc test where appropriate. All statistical analysis were done using Graphpad Prism 8 software. A Welch's t-test or ANOVA were used in cases where variability between groups significantly differed. Statistical significance was set to a $p \leq 0.05$. All values are presented as means ± SEM.

References

1. Mah, J.K., Korngut, L., Dykeman, J., Day, L., Pringsheim, T., and Jette, N. (2014). A systematic review and meta-analysis on the epidemiology of Duchenne and Becker muscular dystrophy. Neuromuscul Disord *24*, 482-491. 10.1016/j.nmd.2014.03.008.
2. Falzarano, M.S., Scotton, C., Passarelli, C., and Ferlini, A. (2015). Duchenne Muscular Dystrophy: From Diagnosis to Therapy. Molecules *20*, 18168-18184. 10.3390/molecules201018168.
3. Laviola, M., Priori, R., D'Angelo, M.G., and Aliverti, A. (2018). Assessment of diaphragmatic thickness by ultrasonography in Duchenne muscular dystrophy (DMD) patients. PLoS One *13*, e0200582. 10.1371/journal.pone.0200582.
4. Cotton, S., Voudouris, N.J., and Greenwood, K.M. (2001). Intelligence and Duchenne muscular dystrophy: full-scale, verbal, and performance intelligence quotients. Dev Med Child Neurol *43*, 497-501. 10.1017/s0012162201000913.
5. Dorman, C., Hurley, A.D., and D'Avignon, J. (1988). Language and learning disorders of older boys with Duchenne muscular dystrophy. Dev Med Child Neurol *30*, 316-327. 10.1111/j.1469-8749.1988.tb14556.x.
6. Beurel, E., Grieco, S.F., and Jope, R.S. (2015). Glycogen synthase kinase-3 (GSK3): regulation, actions, and diseases. Pharmacol Ther *148*, 114-131. 10.1016/j.pharmthera.2014.11.016.
7. Wang, H., Brown, J., and Martin, M. (2011). Glycogen synthase kinase 3: a point of convergence for the host inflammatory response. Cytokine *53*, 130-140. 10.1016/j.cyto.2010.10.009.
8. Leroy, K., and Brion, J.P. (1999). Developmental expression and localization of glycogen synthase kinase-3beta in rat brain. J Chem Neuroanat *16*, 279-293. 10.1016/s0891-0618(99)00012-5.
9. Mirzoev, T.M., Sharlo, K.A., and Shenkman, B.S. (2021). The Role of GSK-3β in the Regulation of Protein Turnover, Myosin Phenotype, and Oxidative Capacity in Skeletal Muscle under Disuse Conditions. Int J Mol Sci *22*, 5081. 10.3390/ijms22105081.
10. Whitley, K.C., Hamstra, S.I., Baranowski, R.W., Watson, C.J.F., MacPherson, R.E.K., MacNeil, A.J., Roy, B.D., Vandenboom, R., and Fajardo, V.A. (2020). GSK3 inhibition with low dose lithium supplementation augments murine muscle fatigue resistance and specific force production. Physiol Rep *8*, e14517. 10.14814/phy2.14517.
11. Pansters, N.A., Schols, A.M., Verhees, K.J., de Theije, C.C., Snepvangers, F.J., Kelders, M.C., Ubags, N.D., Haegens, A., and Langen, R.C. (2015). Muscle-specific GSK-3beta ablation accelerates regeneration of disuse-atrophied skeletal muscle. Biochim Biophys Acta *1852*, 490-506. 10.1016/j.bbadis.2014.12.006.
12. Chakkalakal, J.V., Harrison, M.A., Carbonetto, S., Chin, E., Michel, R.N., and Jasmin, B.J. (2004). Stimulation of calcineurin signaling attenuates the dystrophic pathology in mdx mice. Hum Mol Genet *13*, 379-388. 10.1093/hmg/ddh037.
13. Chakkalakal, J.V., Stocksley, M.A., Harrison, M.A., Angus, L.M., Deschenes-Furry, J., St-Pierre, S., Megeney, L.A., Chin, E.R., Michel, R.N., and Jasmin, B.J. (2003). Expression of utrophin A mRNA correlates with the oxidative capacity of skeletal muscle fiber types and is regulated by calcineurin/NFAT signaling. Proc Natl Acad Sci U S A *100*, 7791-7796. 10.1073/pnas.0932671100.
14. Fajardo, V.A., Chambers, P.J., Juracic, E.S., Rietze, B.A., Gamu, D., Bellissimo, C., Kwon, F., Quadrilatero, J., and Russell Tupling, A. (2018). Sarcolipin deletion in mdx

mice impairs calcineurin signalling and worsens dystrophic pathology. Hum Mol Genet. 10.1093/hmg/ddy302.
15. Chakkalakal, J.V., Michel, S.A., Chin, E.R., Michel, R.N., and Jasmin, B.J. (2006). Targeted inhibition of Ca2+ /calmodulin signaling exacerbates the dystrophic phenotype in mdx mouse muscle. Hum Mol Genet *15*, 1423-1435. 10.1093/hmg/ddl065.
16. Ning, H., Ren, H., Zhao, Y., Yin, H., Gan, Z., Shen, Y., and Yu, Y. (2022). Targeting the DP2 receptor alleviates muscle atrophy and diet-induced obesity in mice through oxidative myofiber transition. J Cachexia Sarcopenia Muscle. 10.1002/jcsm.13136.
17. Cohen, P., and Goedert, M. (2004). GSK3 inhibitors: development and therapeutic potential. Nat Rev Drug Discov *3*, 479-487. 10.1038/nrd1415.
18. Hayward, G.C., Caceres, D., Copeland, E.N., Baranowski, B.J., Mohammad, A., Whitley, K.C., Fajardo, V.A., and MacPherson, R.E.K. (2022). Characterization of Alzheimer's disease-like neuropathology in Duchenne's muscular dystrophy using the DBA/2J mdx mouse model. FEBS Open Bio *12*, 154-162. 10.1002/2211-5463.13317.
19. Salam, E.A., Abdel-Meguid, I.E., Shatla, R., and Korraa, S. (2014). Evaluation of neural damage in Duchenne muscular dystrophy patients. Acta Myol *33*, 13-18.
20. Ly, P.T., Wu, Y., Zou, H., Wang, R., Zhou, W., Kinoshita, A., Zhang, M., Yang, Y., Cai, F., Woodgett, J., and Song, W. (2013). Inhibition of GSK3β-mediated BACE1 expression reduces Alzheimer-associated phenotypes. J Clin Invest *123*, 224-235. 10.1172/jci64516.
21. Khan, I., Tantray, M.A., Alam, M.S., and Hamid, H. (2017). Natural and synthetic bioactive inhibitors of glycogen synthase kinase. Eur J Med Chem *125*, 464-477. 10.1016/j.ejmech.2016.09.058.
22. Noori, M.S., Bhatt, P.M., Courreges, M.C., Ghazanfari, D., Cuckler, C., Orac, C.M., McMills, M.C., Schwartz, F.L., Deosarkar, S.P., Bergmeier, S.C., et al. (2019). Identification of a novel selective and potent inhibitor of glycogen synthase kinase-3. Am J Physiol Cell Physiol *317*, C1289-c1303. 10.1152/ajpcell.00061.2019.
23. Vecchio, L.M., Meng, Y., Xhima, K., Lipsman, N., Hamani, C., and Aubert, I. (2018). The Neuroprotective Effects of Exercise: Maintaining a Healthy Brain Throughout Aging. Brain Plast *4*, 17-52. 10.3233/bpl-180069.
24. Ferry, A., Benchaouir, R., Joanne, P., Peat, R.A., Mougenot, N., Agbulut, O., and Butler-Browne, G. (2015). Effect of voluntary physical activity initiated at age 7 months on skeletal hindlimb and cardiac muscle function in mdx mice of both genders. Muscle Nerve *52*, 788-794. 10.1002/mus.24604.
25. Delacroix, C., Hyzewicz, J., Lemaitre, M., Friguet, B., Li, Z., Klein, A., Furling, D., Agbulut, O., and Ferry, A. (2018). Improvement of Dystrophic Muscle Fragility by Short-Term Voluntary Exercise through Activation of Calcineurin Pathway in mdx Mice. Am J Pathol *188*, 2662-2673. 10.1016/j.ajpath.2018.07.015.
26. MacAulay, K., and Woodgett, J.R. (2008). Targeting glycogen synthase kinase-3 (GSK-3) in the treatment of Type 2 diabetes. Expert Opin Ther Targets *12*, 1265-1274. 10.1517/14728222.12.10.1265.
27. Balasubramaniam, M., Mainali, N., Bowroju, S.K., Atluri, P., Penthala, N.R., Ayyadevera, S., Crooks, P.A., and Shmookler Reis, R.J. (2020). Structural modeling of GSK3β implicates the inactive (DFG-out) conformation as the target bound by TDZD analogs. Scientific Reports *10*, 18326. 10.1038/s41598-020-75020-w.

28. Jones, K., Wei, C., Iakova, P., Bugiardini, E., Schneider-Gold, C., Meola, G., Woodgett, J., Killian, J., Timchenko, N.A., and Timchenko, L.T. (2012). GSK3beta mediates muscle pathology in myotonic dystrophy. J Clin Invest *122*, 4461-4472. 10.1172/JCI64081.
29. Armagan, G., Sevgili, E., Gürkan, F.T., Köse, F.A., Bilgiç, T., Dagcı, T., and Saso, L. (2019). Regulation of the Nrf2 Pathway by Glycogen Synthase Kinase-3β in MPP+-Induced Cell Damage. Molecules *24*. 10.3390/molecules24071377.
30. Kurgan, N., Whitley, K.C., Maddalena, L.A., Moradi, F., Stoikos, J., Hamstra, S.I., Rubie, E.A., Kumar, M., Roy, B.D., Woodgett, J.R., et al. (2019). A Low-Therapeutic Dose of Lithium Inhibits GSK3 and Enhances Myoblast Fusion in C2C12 Cells. Cells *8*. 10.3390/cells8111340.
31. Deconinck, A.E., Rafael, J.A., Skinner, J.A., Brown, S.C., Potter, A.C., Metzinger, L., Watt, D.J., Dickson, J.G., Tinsley, J.M., and Davies, K.E. (1997). Utrophin-dystrophin-deficient mice as a model for Duchenne muscular dystrophy. Cell *90*, 717-727.
32. Grady, R.M., Teng, H., Nichol, M.C., Cunningham, J.C., Wilkinson, R.S., and Sanes, J.R. (1997). Skeletal and cardiac myopathies in mice lacking utrophin and dystrophin: a model for Duchenne muscular dystrophy. Cell *90*, 729-738.
33. Angus, L.M., Chakkalakal, J.V., Mejat, A., Eibl, J.K., Belanger, G., Megeney, L.A., Chin, E.R., Schaeffer, L., Michel, R.N., and Jasmin, B.J. (2005). Calcineurin-NFAT signaling, together with GABP and peroxisome PGC-1{alpha}, drives utrophin gene expression at the neuromuscular junction. Am J Physiol Cell Physiol *289*, C908-917. 10.1152/ajpcell.00196.2005.
34. Little, W.C., Ohno, M., Kitzman, D.W., Thomas, J.D., and Cheng, C.P. (1995). Determination of left ventricular chamber stiffness from the time for deceleration of early left ventricular filling. Circulation *92*, 1933-1939. 10.1161/01.cir.92.7.1933.
35. Hamstra, S.I., Roy, B.D., Tiidus, P., MacNeil, A.J., Klentrou, P., MacPherson, R.E.K., and Fajardo, V.A. (2022). Beyond its psychiatric use: the benefits of low dose lithium supplementation. Curr Neuropharmacol. 10.2174/1570159x20666220302151224.
36. Schiaffino, S., and Reggiani, C. (2011). Fiber types in mammalian skeletal muscles. Physiol Rev *91*, 1447-1531. 10.1152/physrev.00031.2010

91/4/1447 [pii].
37. Mawuenyega, K.G., Sigurdson, W., Ovod, V., Munsell, L., Kasten, T., Morris, J.C., Yarasheski, K.E., and Bateman, R.J. (2010). Decreased clearance of CNS beta-amyloid in Alzheimer's disease. Science *330*, 1774. 10.1126/science.1197623.
38. Winkler, E.A., Sagare, A.P., and Zlokovic, B.V. (2014). The pericyte: a forgotten cell type with important implications for Alzheimer's disease? Brain Pathol *24*, 371-386. 10.1111/bpa.12152.
39. Findlay, A.R., Bengoechea, R., Pittman, S.K., Chou, T.F., True, H.L., and Weihl, C.C. (2019). Lithium chloride corrects weakness and myopathology in a preclinical model of LGMD1D. Neurol Genet *5*, e318. 10.1212/NXG.0000000000000318.
40. Feng, H.L., Leng, Y., Ma, C.H., Zhang, J., Ren, M., and Chuang, D.M. (2008). Combined lithium and valproate treatment delays disease onset, reduces neurological deficits and prolongs survival in an amyotrophic lateral sclerosis mouse model. Neuroscience *155*, 567-572. 10.1016/j.neuroscience.2008.06.040.
41. Group, U.K.-L.S., Morrison, K.E., Dhariwal, S., Hornabrook, R., Savage, L., Burn, D.J., Khoo, T.K., Kelly, J., Murphy, C.L., Al-Chalabi, A., et al. (2013). Lithium in patients with amyotrophic lateral sclerosis (LiCALS): a phase 3 multicentre, randomised, double-

blind, placebo-controlled trial. Lancet Neurol *12*, 339-345. 10.1016/S1474-4422(13)70037-1.
42. Rockenstein, E., Torrance, M., Adame, A., Mante, M., Bar-on, P., Rose, J.B., Crews, L., and Masliah, E. (2007). Neuroprotective effects of regulators of the glycogen synthase kinase-3beta signaling pathway in a transgenic model of Alzheimer's disease are associated with reduced amyloid precursor protein phosphorylation. J Neurosci *27*, 1981-1991. 10.1523/JNEUROSCI.4321-06.2007.
43. Rana, A.K., and Singh, D. (2018). Targeting glycogen synthase kinase-3 for oxidative stress and neuroinflammation: Opportunities, challenges and future directions for cerebral stroke management. Neuropharmacology *139*, 124-136. 10.1016/j.neuropharm.2018.07.006.
44. Potz, B.A., Scrimgeour, L.A., Sabe, S.A., Clements, R.T., Sodha, N.R., and Sellke, F.W. (2018). Glycogen synthase kinase 3β inhibition reduces mitochondrial oxidative stress in chronic myocardial ischemia. J Thorac Cardiovasc Surg *155*, 2492-2503. 10.1016/j.jtcvs.2017.12.127.
45. Tinsley, J., Deconinck, N., Fisher, R., Kahn, D., Phelps, S., Gillis, J.M., and Davies, K. (1998). Expression of full-length utrophin prevents muscular dystrophy in mdx mice. Nat Med *4*, 1441-1444. 10.1038/4033.
46. Kennedy, T.L., Guiraud, S., Edwards, B., Squire, S., Moir, L., Babbs, A., Odom, G., Golebiowski, D., Schneider, J., Chamberlain, J.S., and Davies, K.E. (2018). Micro-utrophin Improves Cardiac and Skeletal Muscle Function of Severely Affected D2/mdx Mice. Mol Ther Methods Clin Dev *11*, 92-105. 10.1016/j.omtm.2018.10.005.
47. Strakova, J., Kamdar, F., Kulhanek, D., Razzoli, M., Garry, D.J., Ervasti, J.M., Bartolomucci, A., and Townsend, D. (2018). Integrative effects of dystrophin loss on metabolic function of the mdx mouse. Scientific Reports *8*, 13624. 10.1038/s41598-018-31753-3.
48. Lin, L., Chen, K., Abdel Khalek, W., Ward, J.L., 3rd, Yang, H., Chabi, B., Wrutniak-Cabello, C., and Tong, Q. (2014). Regulation of skeletal muscle oxidative capacity and muscle mass by SIRT3. PLoS One *9*, e85636. 10.1371/journal.pone.0085636.
49. Matthews, E., Brassington, R., Kuntzer, T., Jichi, F., and Manzur, A.Y. (2016). Corticosteroids for the treatment of Duchenne muscular dystrophy. Cochrane Database Syst Rev *2016*, Cd003725. 10.1002/14651858.CD003725.pub4.
50. Birnkrant, D.J., Bushby, K., Bann, C.M., Apkon, S.D., Blackwell, A., Brumbaugh, D., Case, L.E., Clemens, P.R., Hadjiyannakis, S., Pandya, S., et al. (2018). Diagnosis and management of Duchenne muscular dystrophy, part 1: diagnosis, and neuromuscular, rehabilitation, endocrine, and gastrointestinal and nutritional management. Lancet Neurol *17*, 251-267. 10.1016/s1474-4422(18)30024-3.
51. Weber, D.R., Hadjiyannakis, S., McMillan, H.J., Noritz, G., and Ward, L.M. (2018). Obesity and Endocrine Management of the Patient With Duchenne Muscular Dystrophy. Pediatrics *142*, S43-s52. 10.1542/peds.2018-0333F.
52. Choi, S.E., Jang, H.J., Kang, Y., Jung, J.G., Han, S.J., Kim, H.J., Kim, D.J., and Lee, K.W. (2010). Atherosclerosis induced by a high-fat diet is alleviated by lithium chloride via reduction of VCAM expression in ApoE-deficient mice. Vascul Pharmacol *53*, 264-272. 10.1016/j.vph.2010.09.004.

53. Henriksen, E.J., and Dokken, B.B. (2006). Role of glycogen synthase kinase-3 in insulin resistance and type 2 diabetes. Curr Drug Targets *7*, 1435-1441. 10.2174/1389450110607011435.
54. Pearce, N.J., Arch, J.R., Clapham, J.C., Coghlan, M.P., Corcoran, S.L., Lister, C.A., Llano, A., Moore, G.B., Murphy, G.J., Smith, S.A., et al. (2004). Development of glucose intolerance in male transgenic mice overexpressing human glycogen synthase kinase-3beta on a muscle-specific promoter. Metabolism *53*, 1322-1330. 10.1016/j.metabol.2004.05.008.
55. Coley, W.D., Bogdanik, L., Vila, M.C., Yu, Q., Van Der Meulen, J.H., Rayavarapu, S., Novak, J.S., Nearing, M., Quinn, J.L., Saunders, A., et al. (2016). Effect of genetic background on the dystrophic phenotype in mdx mice. Hum Mol Genet *25*, 130-145. 10.1093/hmg/ddv460.
56. Zhazykbayeva, S., Pabel, S., Mügge, A., Sossalla, S., and Hamdani, N. (2020). The molecular mechanisms associated with the physiological responses to inflammation and oxidative stress in cardiovascular diseases. Biophys Rev *12*, 947-968. 10.1007/s12551-020-00742-0.
57. Bagdatlioglu, E., Porcari, P., Greally, E., Blamire, A.M., and Straub, V.W. (2020). Cognitive impairment appears progressive in the mdx mouse. Neuromuscul Disord *30*, 368-388. 10.1016/j.nmd.2020.02.018.
58. Comim, C.M., Ventura, L., Freiberger, V., Dias, P., Bragagnolo, D., Dutra, M.L., Amaral, R.A., Camargo-Fagundes, A.L.S., Reis, P.A., Castro-Faria-Neto, H.C., et al. (2019). Neurocognitive Impairment in mdx Mice. Mol Neurobiol. 10.1007/s12035-019-1573-7.
59. Remmelink, E., Aartsma-Rus, A., Smit, A.B., Verhage, M., Loos, M., and van Putten, M. (2016). Cognitive flexibility deficits in a mouse model for the absence of full-length dystrophin. Genes Brain Behav *15*, 558-567. 10.1111/gbb.12301.
60. Forlenza, O.V., De-Paula, V.J., and Diniz, B.S. (2014). Neuroprotective effects of lithium: implications for the treatment of Alzheimer's disease and related neurodegenerative disorders. ACS Chem Neurosci *5*, 443-450. 10.1021/cn5000309.
61. Nunes, M.A., Schowe, N.M., Monteiro-Silva, K.C., Baraldi-Tornisielo, T., Souza, S.I., Balthazar, J., Albuquerque, M.S., Caetano, A.L., Viel, T.A., and Buck, H.S. (2015). Chronic Microdose Lithium Treatment Prevented Memory Loss and Neurohistopathological Changes in a Transgenic Mouse Model of Alzheimer's Disease. PLoS One *10*, e0142267. 10.1371/journal.pone.0142267.
62. Ostrovskaya, R.U., Ivanov, S.V., and Durnev, A.D. (2018). Neuroprotective Lithium Salts Protect Pancreatic β-Cells from Damage. Bull Exp Biol Med *165*, 758-762. 10.1007/s10517-018-4259-7.
63. Wilson, E.N., Do Carmo, S., Iulita, M.F., Hall, H., Ducatenzeiler, A., Marks, A.R., Allard, S., Jia, D.T., Windheim, J., and Cuello, A.C. (2017). BACE1 inhibition by microdose lithium formulation NP03 rescues memory loss and early stage amyloid neuropathology. Transl Psychiatry *7*, e1190. 10.1038/tp.2017.169.
64. Yu, F., Zhang, Y., and Chuang, D.M. (2012). Lithium reduces BACE1 overexpression, β amyloid accumulation, and spatial learning deficits in mice with traumatic brain injury. J Neurotrauma *29*, 2342-2351. 10.1089/neu.2012.2449.

65. Chatterjee, S., and Mudher, A. (2018). Alzheimer's Disease and Type 2 Diabetes: A Critical Assessment of the Shared Pathological Traits. Front Neurosci *12*, 383. 10.3389/fnins.2018.00383.
66. Pugazhenthi, S., Qin, L., and Reddy, P.H. (2017). Common neurodegenerative pathways in obesity, diabetes, and Alzheimer's disease. Biochim Biophys Acta Mol Basis Dis *1863*, 1037-1045. 10.1016/j.bbadis.2016.04.017.
67. Yoon, S.S., and Jo, S.A. (2012). Mechanisms of Amyloid-β Peptide Clearance: Potential Therapeutic Targets for Alzheimer's Disease. Biomol Ther (Seoul) *20*, 245-255. 10.4062/biomolther.2012.20.3.245.
68. Deane, R., Wu, Z., and Zlokovic, B.V. (2004). RAGE (yin) versus LRP (yang) balance regulates alzheimer amyloid beta-peptide clearance through transport across the blood-brain barrier. Stroke *35*, 2628-2631. 10.1161/01.STR.0000143452.85382.d1.
69. Horrigan, J., Gomes, T.B., Snape, M., Nikolenko, N., McMorn, A., Evans, S., Yaroshinsky, A., Della Pasqua, O., Oosterholt, S., and Lochmüller, H. (2020). A Phase 2 Study of AMO-02 (Tideglusib) in Congenital and Childhood-Onset Myotonic Dystrophy Type 1 (DM1). Pediatr Neurol *112*, 84-93. 10.1016/j.pediatrneurol.2020.08.001.
70. Baranowski, R.W., Braun, J.L., Vandenboom, R., and Fajardo, V.A. (2022). Neurogranin inhibits calcineurin in murine soleus muscle: Effects of heterozygous knockdown on muscle adaptations to tenotomy and fatigue resistance. Biochemical and Biophysical Research Communications *623*, 89-95. https://doi.org/10.1016/j.bbrc.2022.07.062.
71. Bigard, X., Sanchez, H., Zoll, J., Mateo, P., Rousseau, V., Veksler, V., and Ventura-Clapier, R. (2000). Calcineurin Co-regulates contractile and metabolic components of slow muscle phenotype. J Biol Chem *275*, 19653-19660. 10.1074/jbc.M000430200.
72. Long, Y.C., Glund, S., Garcia-Roves, P.M., and Zierath, J.R. (2007). Calcineurin regulates skeletal muscle metabolism via coordinated changes in gene expression. J Biol Chem *282*, 1607-1614. 10.1074/jbc.M609208200.
73. Talmadge, R.J., Otis, J.S., Rittler, M.R., Garcia, N.D., Spencer, S.R., Lees, S.J., and Naya, F.J. (2004). Calcineurin activation influences muscle phenotype in a muscle-specific fashion. BMC Cell Biol *5*, 28. 10.1186/1471-2121-5-28

1471-2121-5-28 [pii].
74. Fajardo, V.A., Gamu, D., Rietze, B.A., Kwon, F., Chamebrs, P.J., Quadrilatero, J., Tupling, A.R. (2016). Sarcolipin Deletion in mdx mice Worsens Dystrophic Pathology by Impairing Calcineurin Signaling and Reducing Utrophin Expression. FASEB J *30*, 1224.1226.
75. Stupka, N., Schertzer, J.D., Bassel-Duby, R., Olson, E.N., and Lynch, G.S. (2008). Stimulation of calcineurin Aalpha activity attenuates muscle pathophysiology in mdx dystrophic mice. Am J Physiol Regul Integr Comp Physiol *294*, R983-992. 10.1152/ajpregu.00375.2007.
76. Rommel, C., Bodine, S.C., Clarke, B.A., Rossman, R., Nunez, L., Stitt, T.N., Yancopoulos, G.D., and Glass, D.J. (2001). Mediation of IGF-1-induced skeletal myotube hypertrophy by PI(3)K/Akt/mTOR and PI(3)K/Akt/GSK3 pathways. Nat Cell Biol *3*, 1009-1013. 10.1038/ncb1101-1009.
77. Shen, T., Cseresnyes, Z., Liu, Y., Randall, W.R., and Schneider, M.F. (2007). Regulation of the nuclear export of the transcription factor NFATc1 by protein kinases after slow fibre type electrical stimulation of adult mouse skeletal muscle fibres. J Physiol *579*, 535-551. 10.1113/jphysiol.2006.120048.

78. Hammer, S., Toussaint, M., Vollsæter, M., Nesbjørg Tvedt, M., Drange Røksund, O., Reychler, G., Lund, H., and Andersen, T. (2022). Exercise Training in Duchenne Muscular Dystrophy: A Systematic Review and Meta-Analysis. J Rehabil Med *54*, jrm00250. 10.2340/jrm.v53.985.
79. van Putten, M., Putker, K., Overzier, M., Adamzek, W.A., Pasteuning-Vuhman, S., Plomp, J.J., and Aartsma-Rus, A. (2019). Natural disease history of the D2-mdx mouse model for Duchenne muscular dystrophy. FASEB J *33*, 8110-8124. 10.1096/fj.201802488R.
80. Lei, P., Ayton, S., Bush, A.I., and Adlard, P.A. (2011). GSK-3 in Neurodegenerative Diseases. Int J Alzheimers Dis *2011*, 189246. 10.4061/2011/189246.
81. Geromella, M.S., Ryan, C.R., Braun, J.L., Finch, M.S., Maddalena, L.A., Bagshaw, O., Hockey, B.L., Moradi, F., Fenech, R.K., Ryoo, J., et al. (2022). Low-dose lithium supplementation promotes adipose tissue browning and sarco(endo)plasmic reticulum Ca(2+) ATPase uncoupling in muscle. J Biol Chem *298*, 102568. 10.1016/j.jbc.2022.102568.
82. Mendez J, K., A (1960). Density and composition of mammalian muscle. Metabolism *9*, 184-188.
83. Brooks, S.V., and Faulkner, J.A. (1988). Contractile properties of skeletal muscles from young, adult and aged mice. J Physiol *404*, 71-82.
84. Bloemberg, D., and Quadrilatero, J. (2012). Rapid determination of myosin heavy chain expression in rat, mouse, and human skeletal muscle using multicolor immunofluorescence analysis. PLoS One *7*, e35273. 10.1371/journal.pone.0035273

PONE-D-11-20138 [pii].
85. Braun, J.L., Teng, A.C.T., Geromella, M.S., Ryan, C.R., Fenech, R.K., MacPherson, R.E.K., Gramolini, A.O., and Fajardo, V.A. (2021). Neuronatin promotes SERCA uncoupling and its expression is altered in skeletal muscles of high-fat diet-fed mice. FEBS Lett *595*, 2756-2767. 10.1002/1873-3468.14213.
86. Geromella, M.S., Braun, J.L., and Fajardo, V.A. (2023). Measuring SERCA-mediated calcium uptake in mouse muscle homogenates. STAR Protoc *4*, 101987. 10.1016/j.xpro.2022.101987.
87. Fajardo, V.A., Bombardier, E., McMillan, E., Tran, K., Wadsworth, B.J., Gamu, D., Hopf, A., Vigna, C., Smith, I.C., Bellissimo, C., et al. (2015). Phospholamban overexpression in mice causes a centronuclear myopathy-like phenotype. Dis Model Mech *8*, 999-1009. 10.1242/dmm.020859.

Figure 1

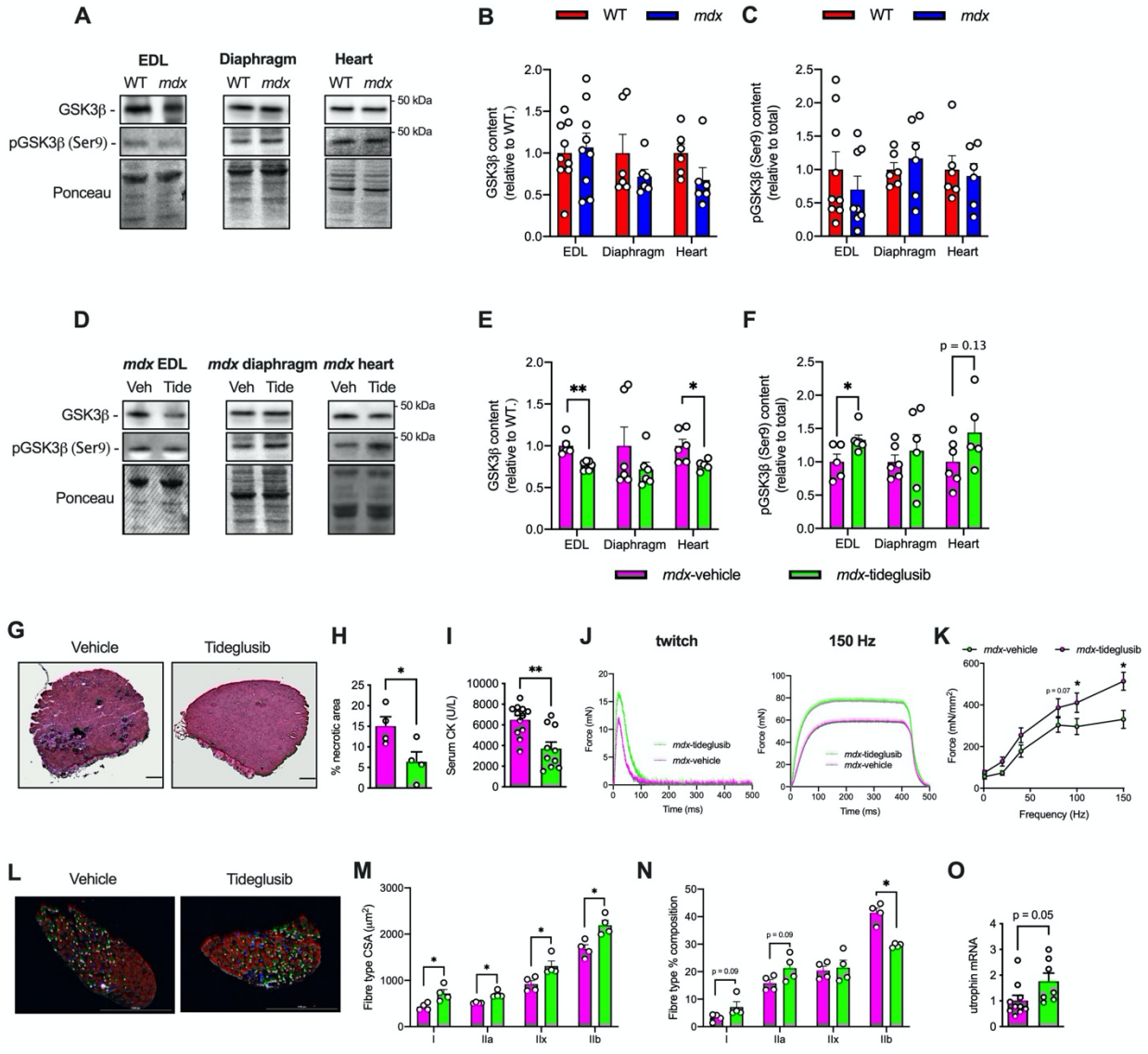
A
EDL
Diaphragm
Heart
WT mdx
GSK3β -
pGSK3β (Ser9) -
Ponceau
50 kDa
B
WT
mdx
GSK3β content (relative to WT.)
EDL
Diaphragm
Heart
C
pGSK3β (Ser9) content (relative to total)
D
mdx EDL
mdx diaphragm
mdx heart
Veh Tide
E
F
p = 0.13
mdx-vehicle
mdx-tideglusib
G
Vehicle
Tideglusib
H
% necrotic area
I
Serum CK (U/L)
J
twitch
150 Hz
Force (mN)
Time (ms)
K
Force (mN/mm²)
Frequency (Hz)
L
M
Fibre type CSA (µm²)
I
IIa
IIx
IIb
N
Fibre type % composition
p = 0.09
O
utrophin mRNA
p = 0.05

Figure 2

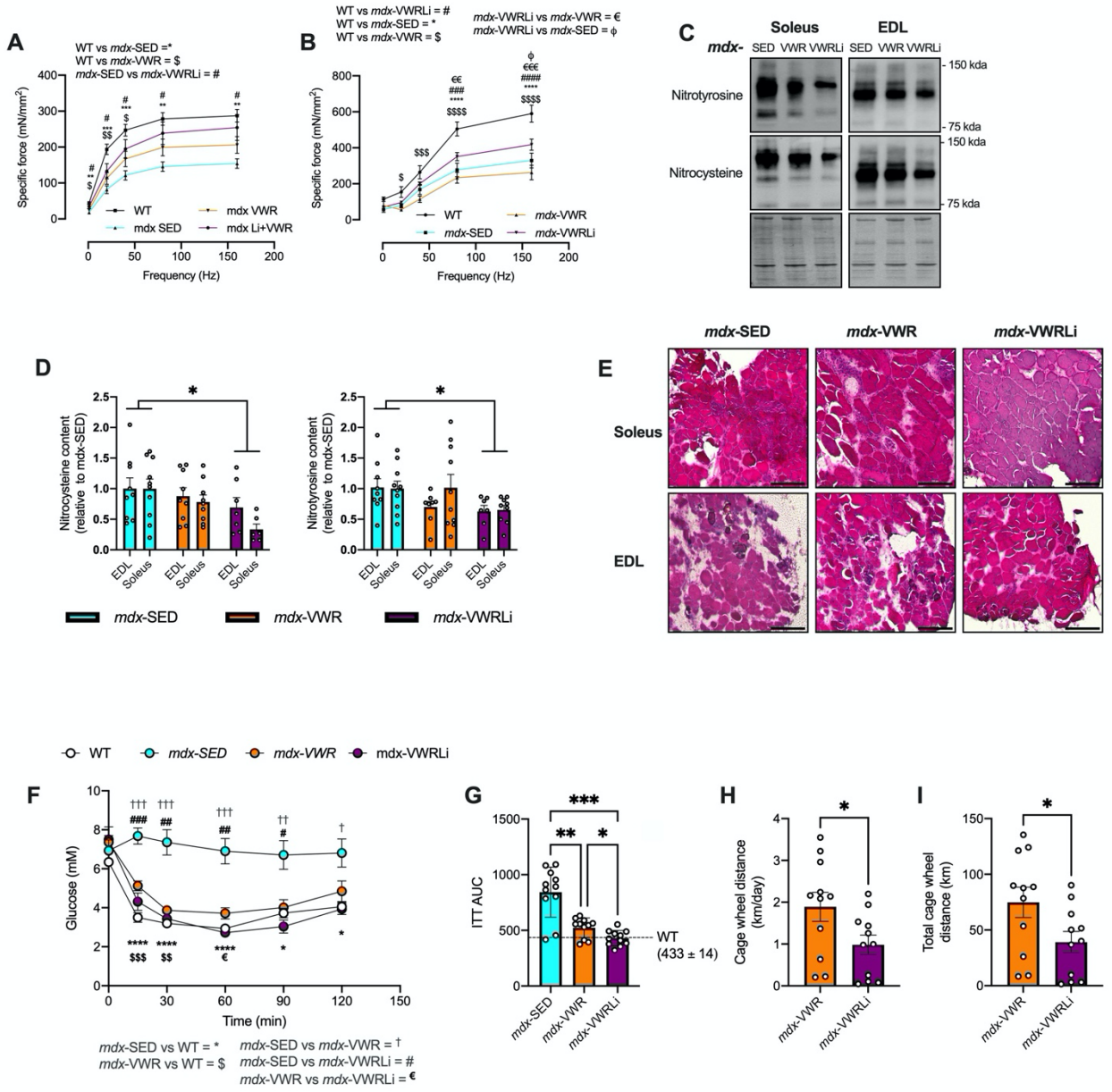
A
WT vs mdx-SED =*
WT vs mdx-VWR = $
mdx-SED vs mdx-VWRLi = #
Specific force (mN/mm²)
Frequency (Hz)
WT
mdx VWR
mdx SED
mdx Li+VWR
B
WT vs mdx-VWRLi = #
WT vs mdx-SED = *
WT vs mdx-VWR = $
mdx-VWRLi vs mdx-VWR = €
mdx-VWRLi vs mdx-SED = ϕ
Specific force (mN/mm²)
Frequency (Hz)
WT
mdx-VWR
mdx-SED
mdx-VWRLi
C
Soleus
EDL
mdx-
SED VWR VWRLi SED VWR VWRLi
Nitrotyrosine
Nitrocysteine
150 kda
75 kda
150 kda
75 kda
D
Nitrocysteine content (relative to mdx-SED)
Nitrotyrosine content (relative to mdx-SED)
EDL
Soleus
mdx-SED
mdx-VWR
mdx-VWRLi
E
mdx-SED
mdx-VWR
mdx-VWRLi
Soleus
EDL
WT
mdx-SED
mdx-VWR
mdx-VWRLi
F
Glucose (mM)
Time (min)
mdx-SED vs WT = *
mdx-VWR vs WT = $
mdx-SED vs mdx-VWR = †
mdx-SED vs mdx-VWRLi = #
mdx-VWR vs mdx-VWRLi = €
G
ITT AUC
WT
(433 ± 14)
mdx-SED
mdx-VWR
mdx-VWRLi
H
Cage wheel distance (km/day)
mdx-VWR
mdx-VWRLi
I
Total cage wheel distance (km)
mdx-VWR
mdx-VWRLi

Figure 3

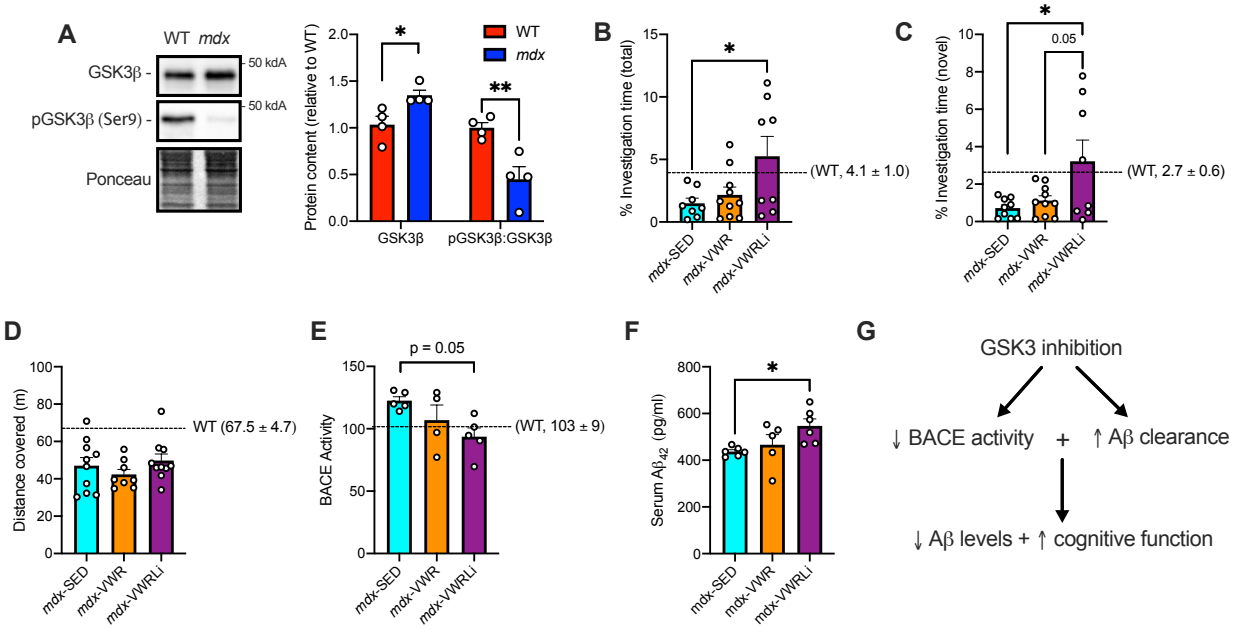
A
WT mdx
GSK3β -
pGSK3β (Ser9) -
Ponceau
50 kDA
50 kDA
Protein content (relative to WT)
WT
mdx
GSK3β
pGSK3β:GSK3β
B
% Investigation time (total)
(WT, 4.1 ± 1.0)
mdx-SED
mdx-VWR
mdx-VWRLi
C
% Investigation time (novel)
0.05
(WT, 2.7 ± 0.6)
D
Distance covered (m)
WT (67.5 ± 4.7)
E
BACE Activity
p = 0.05
(WT, 103 ± 9)
F
Serum Aβ42 (pg/ml)
G
GSK3 inhibition
↓ BACE activity + ↑ Aβ clearance
↓ Aβ levels + ↑ cognitive function